

Mimicking Localized Surface Plasmons with Structural Dispersion

Zhuo Li,* Liangliang Liu, Antonio I. Fernández-Domínguez, Jianfeng Shi, Changqing Gu, Francisco J. García-Vidal,* and Yu Luo*

One major obstacle in developing plasmonic devices is dissipative loss. Structural waveguide dispersion offers a route to tackle this problem. Although long range propagation of surface waves using this concept is recently reported, experimental realizations of localized surface plasmon resonances with suppressed dissipative loss still remain elusive. In this paper, effective localized surface plasmons in a bounded waveguide filled with only positive dielectrics are modeled theoretically and demonstrated experimentally. Theoretical analysis based on cylindrical wave expansion shows that the effective surface modes are induced by structural dispersion of transverse electric modes. Owing to dramatically suppressed metallic loss, the designed structure can support multipolar sharp plasmonic resonances, which are difficult to attain with natural plasmons at optical frequencies. To probe the characteristics of these resonances in the experiment, a deep-subwavelength open resonator is fabricated and the transmission spectrum at the boundary of the structure is measured. The results reveal that structured-dispersion-induced localized surface plasmons are quite sensitive to the background refractive index but relatively robust to the size and shape of the resonator. These findings open up a new avenue for designer localized surface waves at low frequencies and may find applications in miniaturization of microwave resonators, filters, and terahertz biosensors.

applications in miniaturization of photonic circuits, near-field optics, surface-enhanced spectroscopy, plasmonic antennas and photovoltaics, among others.^[1] Conventional SPPs and LSPs occur at the interface between two materials whose real parts of permittivities have opposite signs, for instance, metal/dielectric interfaces at optical frequencies. In this frequency range, however, large dissipative losses are generally expected, which severely limit the performance of these metal-based plasmonic devices. Particularly, when light impinges on deep subwavelength metal nanoparticles, high order sharp LSPs resonances are usually suppressed. On the other hand, metallic losses decrease towards low frequencies and metals behave akin to perfect electric conductors, which screen out electric fields. Consequently, metal/dielectric interfaces do not support surface plasmons at mid-infrared frequencies and below. To mimic the exotic properties of optical plasmons at low frequencies, the concept of spoof surface plasmon polaritons was introduced by Pendry et al.

1. Introduction

In the past few decades, surface plasmon polaritons (SPPs) and localized surface plasmons (LSPs) have aroused a great deal of interest owing to their superb field-confinement and -enhancement performance in the optical regime.^[1–9] They have found

in 2004.^[10] Since then, a number of efforts have been made to realize low-frequency plasmonics and to explore its applications.^[11–34] In 2012, this concept was extended to LSPs and a corrugated PEC cylinder has been shown to exhibit similar scattering characteristics as a Drude metal rod.^[11] Although spoof LSPs can mimic their natural counterparts in some aspects

Prof. Z. Li, Dr. J. Shi, Prof. C. Gu
Key Laboratory of Radar Imaging and Microwave Photonics
Ministry of Education
College of Electronic and Information Engineering
Nanjing University of Aeronautics and Astronautics
Nanjing 211106, P. R. China
E-mail: lizhuo@nuaa.edu.cn

Prof. Z. Li, Dr. L. Liu, Prof. Y. Luo
School of Electrical and Electronic Engineering
Nanyang Technological University
Nanyang Avenue 639798, Singapore
E-mail: luoyu@ntu.edu.sg

 The ORCID identification number(s) for the author(s) of this article can be found under <https://doi.org/10.1002/adom.201900118>.

Prof. Z. Li
School of Electronic and Information Engineering
Nanjing University of Information Science and Technology
Nanjing 210044, P. R. China

Dr. A. I. Fernández-Domínguez, Prof. F. J. García-Vidal
Departamento de Física Teórica de la Materia Condensada
and Condensed Matter Physics Center (IFIMAC)
Universidad Autónoma de Madrid
E-28049 Madrid, Spain
E-mail: fj.garcia@uam.es

Prof. F. J. García-Vidal
Donostia International Physics Center (DIPC)
E-20018 Donostia/San Sebastian, Spain

DOI: 10.1002/adom.201900118

(e.g., enhanced scattering efficiency and large field enhancements^[11,31]), they are not perfect low-frequency analogues of their optical version. This is because the effective permittivity of two dimensional (2D) corrugated conductors is not negative and spoof LSPs do not decay spatially in the metallic corrugations but resonate along the radial direction. As a result, the resonance properties of these modes rely heavily on the geometry (e.g., the groove depth) of the structure, making many interesting properties of natural LSPs still elusive at low frequencies. Alternatively, it has been shown that low-frequency plasmonics can also be realized with structured dispersion in bounded waveguides.^[35–37] Recently, in a couple of scenarios,^[35–38] this approach has been successfully applied to mimic propagating SPPs exhibiting spatial decay on both sides of the interface.

In this work, we exploit the structural dispersion of transverse electric (TE) modes in a bounded dielectric waveguide to realize effective localized surface plasmons (ELSPs). Specifically, we investigate the physical mechanism behind ELSPs and show how sharp multipolar ELSP resonances can arise when a TE₁ wave impinges on an air cylinder surrounded by a series of metallic thin wires along its perimeter and located in a dielectric-filled parallel-plate waveguide (PPW). Within a certain range of the spectrum, the effective permittivity of the air cylinder becomes negative and multipolar resonances arise, resembling the LSPs supported by a finite metal cylinder at optical frequencies. The resonance condition is derived using cylindrical wave expansion and then compared against COMSOL MULTIPHYSICS simulations and experimental measurements. Our results clearly show that ELSPs give rise to remarkable field enhancements (FEs) at the structure surface, with spatial decay on both sides. More interestingly, as we shrink the diameter of the air cylinder down to deep subwavelength scales, the resonance frequencies of all the modes blueshift and degenerate into a single one where the quasistatic limit is reached and the dipolar ELSP dominates. To verify our theoretical model experimentally, we design a deep subwavelength open ELSP resonator by switching the medium inside and outside the cylinder and cutting the two metal plates into two disks just covering them into the two ends of the cylinder. Numerical and experimental results demonstrate that ELSPs modes are quite sensitive to the background refractive index but relatively robust to the size and shape of the resonator. To the best of our knowledge, this work is the first experimental demonstration of effective localized plasmon resonances in the framework of structured dispersion. It provides an alternative route to realize high-Q electromagnetic resonances at the very deep subwavelength scale.

2. Theoretical Analysis in Bounded Waveguide Structures

Let us begin by revisiting a conventional PPW shown in **Figure 1a**, which is filled with an isotropic and homogeneous dielectric of relative permittivity ϵ_{r1} and relative permeability $\mu_r = 1$. A cylinder with radius a and height d is cut off and filled with another isotropic and homogeneous dielectric of relative permittivity ϵ_{r2} and relative permeability $\mu_r = 1$. To suppress the fundamental TEM mode, an array of metallic wires is placed at the boundary of the two dielectrics. Hence, within the frequency range of interest, the PPW supports only TE₁

mode and the whole structure can be described as an effective medium. The propagation constant β of the TE₁ mode in a dielectric-filled PPW can be expressed as $\beta = \sqrt{k^2 - k_c^2} = \sqrt{k^2 - (\frac{\pi}{d})^2}$, in which $k = k_0 \sqrt{\epsilon_r}$ is the wave number in the dielectric with relative permittivity ϵ_r and $k_c = \frac{\pi}{d}$ is the cutoff wave number in the z -direction. When $k > k_c$, β is real and the TE₁ mode is propagating. When $k < k_c$, β is imaginary and the TE₁ mode becomes evanescent. If we define the relative permittivity of the effective dielectric filling in the waveguide corresponding to the TE₁ mode as $\epsilon_e = \epsilon_r - \frac{\lambda_0^2}{4d^2}$ (λ_0 is the operating wavelength), the wave number in the effective dielectric is $k_e = k_0 \sqrt{\epsilon_e}$. From the effective medium perspective, ϵ_e can be tuned to be either positive or negative, mimicking real dielectrics or metals in the optical regime. In the following part, we show through analytical derivations that it is possible to realize structural dispersion induced ELSPs within a certain frequency regime at the interface between two effective dielectrics with permittivities of opposite signs in their real part ($\text{Re}(\epsilon_{e1}) \cdot \text{Re}(\epsilon_{e2}) < 0$, in which $\epsilon_{ei} = \epsilon_n - \frac{\lambda_0^2}{4d^2}$, $i=1, 2$). And two types of ELSPs resembling a metallic rod in a dielectric or a dielectric inclusion in metallic structures in the optical regime are discussed in detail.

First, to mimic a circular metallic rod immersed in a dielectric in the optical regime, it is imperative that $\epsilon_{e1} > 0$ and $\epsilon_{e2} < 0$. Therefore, the resonance frequencies of the ELSPs must be higher than $\omega_1 = \omega_{\text{cutoff}}|_{\text{TE}_1, \epsilon_{r1}} = \frac{\pi c}{d \sqrt{\text{Re}(\epsilon_{r1})}}$ and lower than $\omega_a = \frac{\pi c}{d} \sqrt{\frac{2}{\text{Re}(\epsilon_{r1} + \epsilon_{r2})}}$, in which ω_1 is the cutoff frequency of the TE₁ mode in a PPW filled with the dielectric of relative permittivity ϵ_{r1} and ω_a is the asymptotic frequency of the SPPs that are supported at the interface between two semi-infinite dielectrics with permittivities ϵ_{e1} and ϵ_{e2} . To probe these plasmonic resonances, we impose a TE₁ incident wave (\vec{E} pointing along the y -direction) propagating along the $-x$ axis within the PPW. On the middle plane (see **Figure 1b**), the electric and magnetic TE₁ fields have only y and z components, respectively, mimicking a plane wave. Thus, we can apply the metamaterial approximation to derive the following analytical expression for the 2D scattering cross-section (SCS) σ_{sc} of the dielectric cylinder in **Figure 1b**

$$\sigma_{\text{sc}} = \frac{4c}{\omega \sqrt{\epsilon_{e1}}} \sum_{n=-\infty}^{\infty} |a_n|^2 \quad (1)$$

where

$$a_n = j^{-n} \frac{\sqrt{\frac{\epsilon_{e1}}{\epsilon_{e2}}} J_n(\beta_1 a) J'_n(\beta_2 a) - J'_n(\beta_1 a) J_n(\beta_2 a)}{H_n^{(2)}(\beta_1 a) J_n(\beta_2 a) - \sqrt{\frac{\epsilon_{e1}}{\epsilon_{e2}}} J'_n(\beta_2 a) H_n^{(2)}(\beta_1 a)} \quad (2)$$

in which $\beta_1 = \beta_0 \sqrt{\epsilon_{e1}}$, $\beta_2 = \beta_0 \sqrt{\epsilon_{e2}}$, J_n is the Bessel function of first kind and order n and $H_n^{(2)}$ is the Hankel function of second kind and order n . The prime means differentiation with respect to the argument in parenthesis. If ϵ_{r1} , ϵ_{r2} , d , and a are all fixed, the resonance characteristics of multipolar ELSPs can be determined analytically by the SCS spectrum using Equation (1) or simply

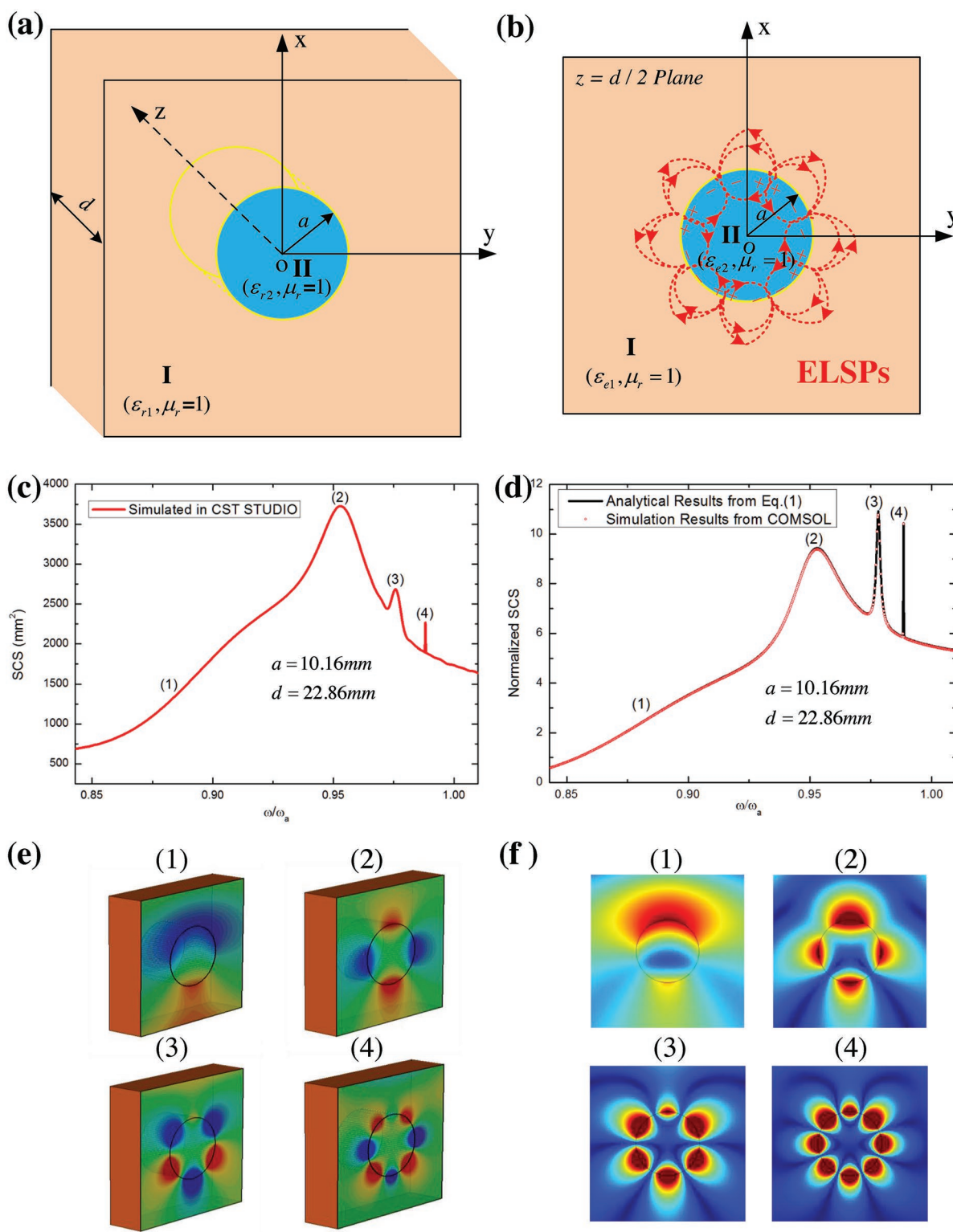


Figure 1. a) A conventional PPW with the separation d between the two plates. Region I is filled with an isotropic and homogeneous dielectric ($\epsilon_{r1}, \mu_r = 1$) and Region II is a cylinder with radius a filled with another isotropic and homogeneous dielectric ($\epsilon_{r2}, \mu_r = 1$). The interface (solid yellow line) is supposed to support structural dispersion induced ELSPs. b) Schematic drawing of the ELSPs supported at the interface between two effective dielectrics with material parameters ($\epsilon_{e1}, \mu_r = 1$) and ($\epsilon_{e2}, \mu_r = 1$) on the $z = d/2$ plane. c) Simulated SCS spectrum (see below) of an air cylinder in a conventional dielectric-filled PPW with $\epsilon_{e1} = 4 - \frac{\lambda_0^2}{4d^2}$ and $\epsilon_{e2} = 1 - \frac{\lambda_0^2}{4d^2}$. d) 2D normalized SCS spectrum of an air disk with $\epsilon_{e1} = 4 - \frac{\lambda_0^2}{4d^2}$ and $\epsilon_{e2} = 1 - \frac{\lambda_0^2}{4d^2}$. e) The magnetic field H_z at the $z = d/2$ plane at four resonances in (c). f) The absolute magnetic field $|H|$ at four resonances in (d).

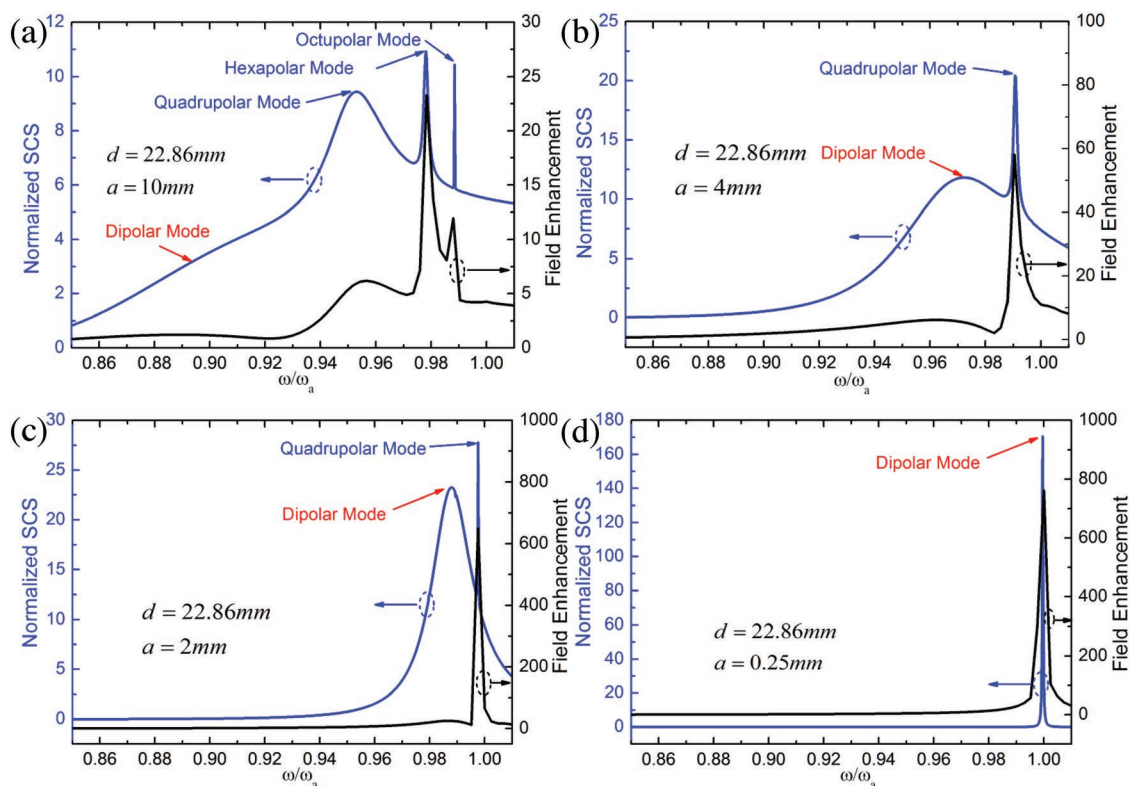


Figure 2. Normalized SCS and FE spectra with the decrease of a) $a = 10$ mm, b) $a = 4$ mm, c) $a = 2$ mm, and d) $a = 0.25$ mm.

calculated from the zeros of the denominator in Equation (2). For a specific case when $\epsilon_{r1} = 4$, $\epsilon_{r2} = 1$, $d = 22.86$ mm and $a = 10.16$ mm, we can obtain $\omega_1 = 2\pi \times (3.28 \times 10^9)$ rad s⁻¹ and $\omega_a = 2\pi \times (4.15 \times 10^9)$ rad s⁻¹. The analytical normalized SCS ($\sigma_{sc}/2a$) spectrum is shown as the black solid line in Figure 1d with the frequency normalized to the asymptotic frequency ω_a . For validations, we also plot the simulated result (the red dotted circle in Figure 1d) obtained from COMSOL MULTIPHYSICS, which is in excellent agreement with the above analytical one. The absolute magnetic fields $|H|$ at four resonances peaks situated at 3.657, 3.955, 4.059, and 4.102 GHz are also shown in Figure 1f, in which we can observe great FEs at the interface with real spatial decay on both sides. It is clear that these four peaks correspond to the di-, quadru-, hexa-, and octupolar ELSPs resonances, respectively.

Contrary to conventional LSPs in the optical regime, spoof LSPs cannot reach the quasistatic limit (in which only the dipolar mode is radiatively active) by scaling down the structure into the subwavelength regime. As a difference, here we show theoretically that ELSPs can mimic real LSPs in their modal evolution simply by shrinking the radius a into the deep subwavelength scale. Figure 2a–d shows that the resonance frequencies of all the ELSPs blueshift and degenerate into a single SCS peak where the dipolar mode dominates over higher-order resonances, and the quasistatic limit is reached. We can derive the resonance condition in the limit $a \rightarrow 0$ from Equation (2), obtaining $\epsilon_{c2} = -\epsilon_{c1}$ for the dipolar ELSP, which recovers the well-known Fröhlich condition for conventional LSPs. Therefore, ELSPs resemble LSPs not only in field distributions but also in their modal evolution. We also plot in Figure 2 the peak FEs on the surface of the cylinder and find that FE at the dipolar resonance increases

with shrinking structural dimensions and reaches a value >800 when the radius a of the structure reduces below 2 mm. These results clearly show the superb field enhancement capabilities of the ELSPs as compared with previous approaches.

Second, in order to mimic a dielectric inclusion in metallic structures in the optical regime, it is imperative that $\epsilon_{c1} < 0$ and $\epsilon_{c2} > 0$. We can simply switch the materials in Regions I and II of Figure 1a by carrying out the substitutions $\epsilon_{r1} \rightarrow \epsilon_{r2}$, $\epsilon_{r2} \rightarrow \epsilon_{r1}$. In this case, the interface is expected to support void plasmons-like ELSPs whose resonance frequencies are also between ω_1 and ω_a . For the specific case $\epsilon_{r1} = 1$, $\epsilon_{r2} = 4$, $d = 22.86$ mm, and $a = 10.16$ mm, the first four resonance frequencies corresponding to the di-, quadru-, hexa-, and octupolar modes can still be calculated from the zeros of the denominator of Equation (2), obtaining 3.734, 3.986, 4.075, and 4.104 GHz, respectively. The evolution of these ELSPs modes with the shrinking size a to deep subwavelength scale is very much like the above, again all modes degenerate into the dipolar resonance in the quasistatic limit.

3. Design and Implementation in Free Space

In our three-dimensional (3D) design, we set the radius of metallic wires around the air cylinder as $d/200$ and the distance between adjacent wires as $d/40$. By imposing a plane wave propagating along the $-x$ direction with the electric field pointing to the y -axis and applying open boundaries at x_{min}/x_{max} , y_{min}/y_{max} , and PEC boundaries at z_{min}/z_{max} , the y -direction polarized incident plane wave naturally becomes TE₁ wave in the waveguide. Thus, we can calculate 3D SCS spectra using the commercial

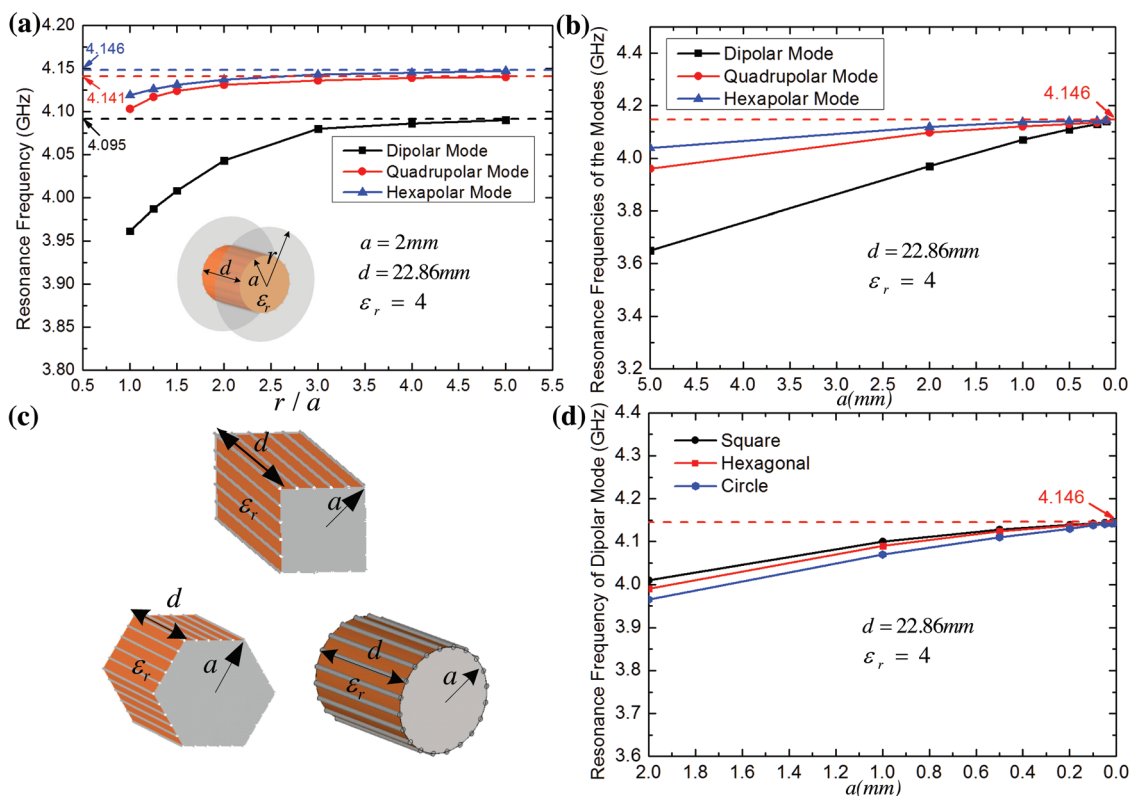


Figure 3. a) Evolution of the resonance frequencies of the di-, quadru-, and hexapolar modes with the variations of the radius ratio r/a ($a = 2\text{ mm}$). The black, red, and blue dashed lines denote the theoretically predicted resonance frequencies of the di-, quadru-, and hexapolar modes when $r \rightarrow \infty$. b) Evolution of the resonance frequencies of the di-, quadru-, and hexapolar modes with the decrease of the radius a from 5 mm down to 0.1 mm. The red dashed line denotes the theoretically predicted frequency for the dipolar ELSP using the quasistatic approximation, $f = c\sqrt{2/\text{Re}(\epsilon_r + 1)}/(2d)$. c) Resonator models with square, hexagonal, and circular cross-section shapes. d) The evolution of the dipolar mode frequency for resonators with different cross-section shapes and against the decrease of a from 2 mm down to 0.01 mm.

software CST STUDIO, as illustrated in Figure 1c. Figure 1e shows the z component of magnetic field H_z at four resonance peaks situated at 3.652, 3.953, 4.055, and 4.1 GHz in the plane $z = d/2$. These four peaks correspond to the di-, quadru-, hexa-, and octupolar ELSPs, which agree with those obtained from the analytical and simulated results for the 2D geometry (see Figure 1d), further demonstrating that we can use the theory above to predict the resonance frequencies for the original 3D structure.

To implement the ELSPs in real applications, we built an open ELSP resonator by switching the materials in- and out-side the cylinder and shrinking the two metallic PPW plates into two finite metallic disks with radius r , as shown in the inset of Figure 3a. A series of metallic wires (with radius $d/200$ and length d) are placed around the perimeter of the dielectric cylinder connecting the two disks. The radius and length of the resonator are set to $a = 2\text{ mm}$, $d = 22.86\text{ mm}$, and the relative permittivities of the dielectrics in- and out-side the resonator are chosen to be $\epsilon_{r2} = 4$ and $\epsilon_{r1} = 1$, respectively. The evolution of the resonance frequencies for the di-, quadru-, and hexapolar modes with r are obtained by using the eigenmode solver in CST STUDIO. They are shown as the black, red, and blue lines in Figure 3a). We can observe that as the ratio r/a increases, the resonance frequencies of all three modes approach theoretical predictions using Equation (2), plotted by dashed lines. Specifically, when r/a exceeds 3, the discrepancies are negligible. Although some deviations due to truncation effects

are observed, one can reasonably use Equation (2) to predict the modal frequencies for an open ELSPs resonator. We also investigate the modal evolution for this open resonator when its radius, a , shrinks into the deep subwavelength scale. Specifically, we plot in Figure 3b) the frequencies of the di-, quadru-, and hexapolar modes against the radius a between 5 mm down to 0.1 mm. We can observe that these three modes degenerate into the dipolar one, and we can use the quasistatic approximation to predict the resonance frequency of this ELSP. Additionally, the evolution of the resonance frequencies of similar modes supported by resonators with square, hexagonal, and circular cross-sections (and the same length shown in Figure 3c) is depicted in the inset of Figure 3d). We find that the ELSP dipolar mode is very robust to variations of resonator cross-section shape in the subwavelength scale.

Consequently, we designed a compact open ELSPs resonator, shown in Figure 4a, which is actually a dielectric cylinder (with radius a and length d) sandwiched between two metallic disks of radius a . Figure 4b) displays three resonator samples with the same cross-section and different lengths. The simulated resonance frequencies of the first three modes (di-, quadru-, and hexapolar modes), 3.962, 4.103, and 4.119 GHz are very close to the theoretical predictions, 4.095, 4.141, and 4.146 GHz. Figure 4c–e) displays the electric field lines and the z component of magnetic field H_z for these three ELSPs, showing that the electric and magnetic fields decay on both sides of the interface.

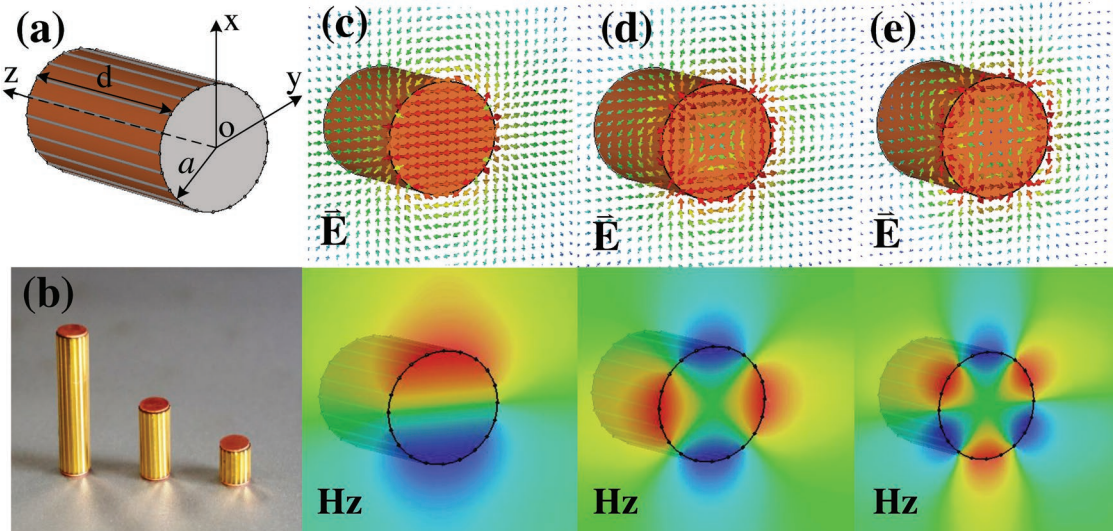


Figure 4. a) Schematic drawing of an open ELSPs resonator. b) ELSP resonator samples. Electric field lines and the z component of magnetic field H_z for the first three ELSP-like modes in the resonator middle plane ($z = d/2$). c) Dipolar mode, d) quadrupolar mode, and e) hexapolar mode.

To further demonstrate the remarkable field enhancement capability of ELSPs over previous approaches, we simulate the electric field at the center of the gap between two open ELSP resonators. A sketch of the system is shown in **Figure 5a**, where the two resonators are characterized by the radius a , height d , and separation s . To compare with Figure 4 in ref. [11], a/d is chosen to be much less than 1 so that each resonator exhibits sharp peak at the dipolar

resonance. The incident wave is x -polarized and propagating along the $-y$ direction. Figure 5b plots the FE as a function of separation evaluated at the dipolar resonance of the dimer system. A dramatic increase in FE is clearly observed for decreasing separation from $s/a = 0.5$ down to $s/a = 0.1$ shown in Figure 5c,d. It is worth noting that the FE in our system is significantly larger than those in previous studies^[11,31] at the same separation-to-radius ratio s/a .

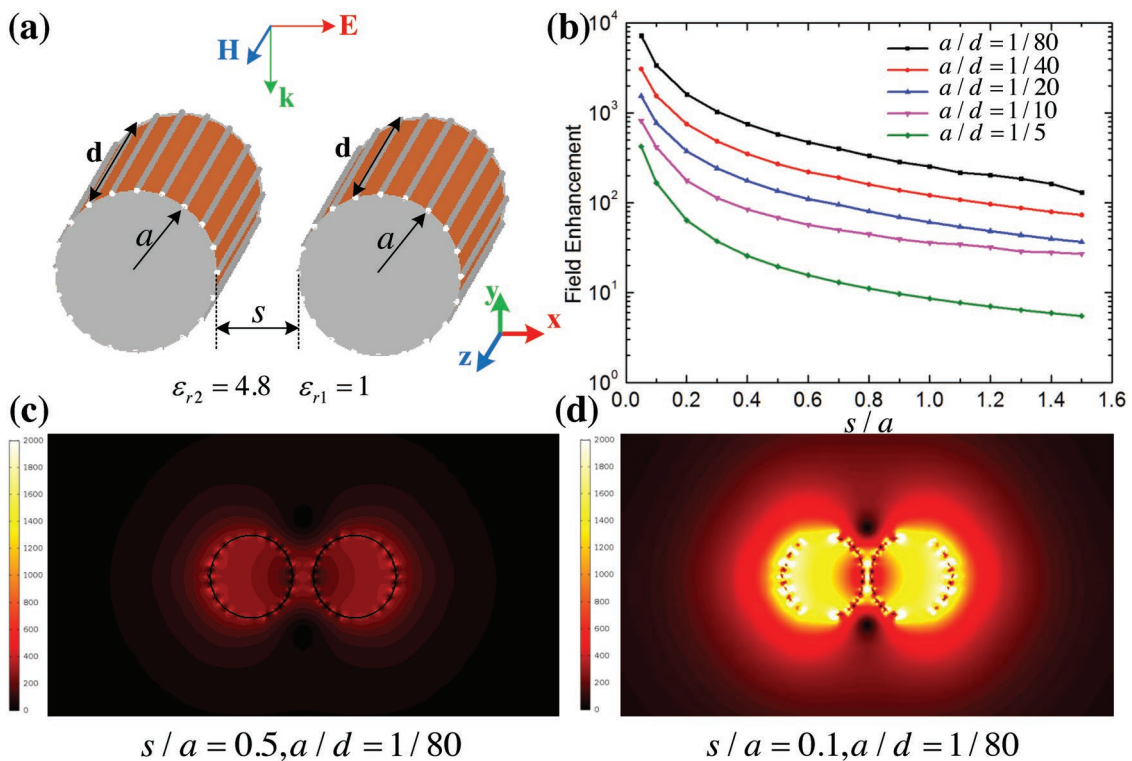


Figure 5. a) 3D open ELSP resonators with radius a , height d , and separation s . The incident plane wave is x -polarized and propagating along the $-y$ direction. b) Electric field enhancements at the center of the gap as a function of the separation between two resonators. c) Field enhancements in the $x-y$ plane for $a/d = 1/80$ when $s/a = 0.5$. d) Field enhancements in the $x-y$ plane for $a/d = 1/80$ when $s/a = 0.1$.

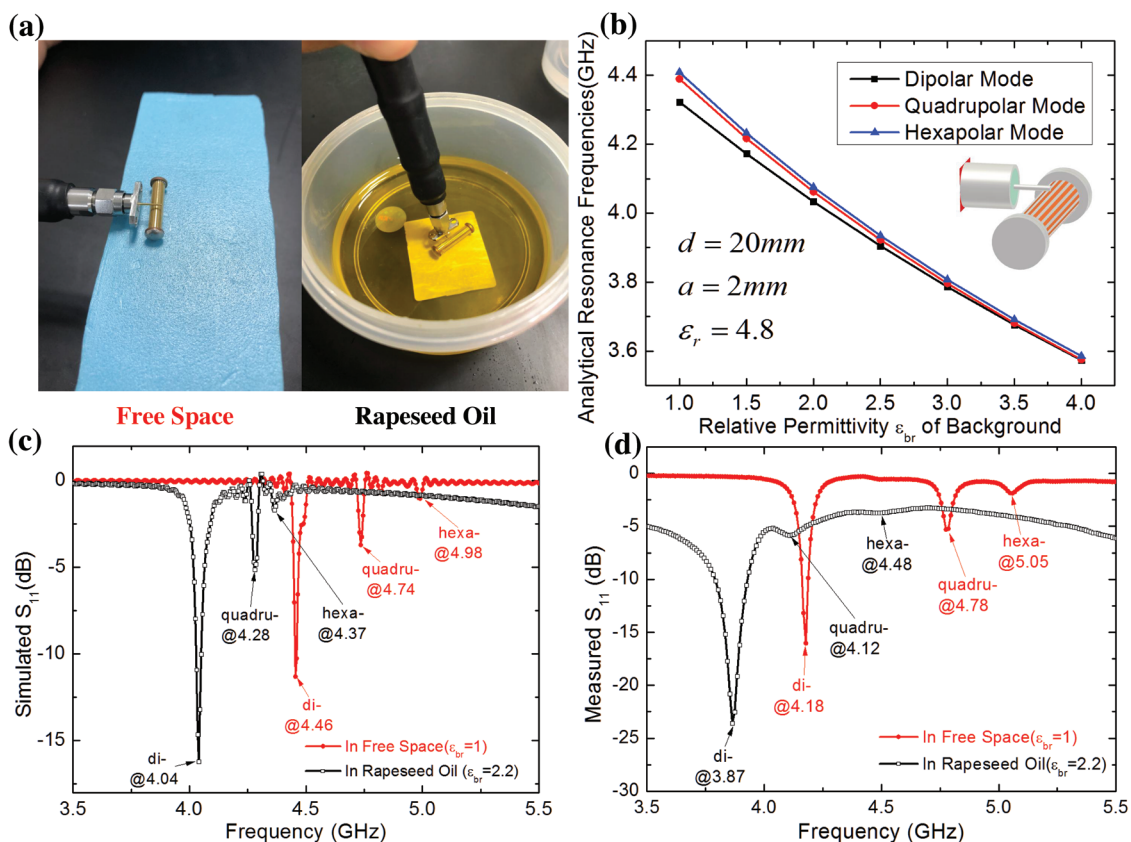


Figure 6. a) Measurements of reflection spectra of the resonator in free space and immersed in rapeseed oil. b) The evolution of the analytical resonance frequencies with the increase of ϵ_{br} . c) Simulated reflection spectra of di-, quadru-, and hexapolar ELSPs. d) Measured reflection spectra of di-, quadru-, and hexapolar ELSPs.

4. Experimental Measurement

To further validate our theoretical results, we choose one of our resonator samples, shown in **Figure 6a**, and probe its ELSP modal characteristics. This resonator is composed of three parts: an F4BM (a woven-glass PTFE substrate with a wide range of dielectric constant) dielectric cylinder (with radius $a = 2\text{ mm}$, length $d = 20\text{ mm}$, relative permittivity $\epsilon_{r2} = 4.8$), a flexible printed circuit (with the thickness of 0.025 mm), and a series of copper strips (with the thickness of 0.018 mm) printed on it and two circular copper disks (with radius $a = 2\text{ mm}$ and thickness of 0.3 mm). The flexible printed circuit is first wrapped around the dielectric cylinder and then soldered to the two copper disks at the two ends of the cylinder to ensure that each metallic strip is in contact with them. For comparison, we also build a simulation model in CST STUDIO shown as the inset in **Figure 6b** and obtain the reflection spectrum of the resonator by positioning a coaxial probe with the inner conductor 2 mm above the middle of, and perpendicular to, the resonator. In **Figure 6c**, the simulated reflection spectrum in free space (red curve) and in rapeseed oil (black curve) show three resonance dips corresponding to the di-, quadru-, and hexapolar modes, respectively. The rapeseed oil (produced in Wuhan, China) typically contains palmitic (4%), stearic (2%), oleic (62%), linoleic (22%), and linolenic (10%) acids. We remark that in the simulations, we

just simply set the permittivity of the background media as $\epsilon_{br} = 1$ and $\epsilon_{br} = 2.2$ without loss mimicking the free space and rapeseed oil. The evolution of the analytical resonance frequencies with the increase of ϵ_{br} are calculated using Equation (2), and are shown in **Figure 6b**. We find that the higher the ϵ_{br} , the lower the resonance frequencies of three ELSP modes. In the experiment, the modal characteristics of the resonator are captured with a coaxial probe connected to one of the test cables of an N5230C vector network analyzer. The measured reflection spectra are shown in **Figure 6d**, where we can also clearly observe three ELSP dips. Although there exists some discrepancies due to the material and fabrication tolerances, as well as the loss not considered in the simulations, these experimental results verify the validity and accuracy of our theory. They also demonstrate that ELSP-based resonators are quite sensitive to variations in their surrounding material, and therefore can be fully utilized as potential sensors. From our analysis, the theoretical resonance frequency for the dipolar ELSP mode using the quasistatic approximation, $f = c\sqrt{2/\text{Re}(\epsilon_r + 1)}/(2d)$, is independent of a , the radius of the resonator. Thus, theoretically, one can arbitrarily shrink down the resonator's diameter without altering the resonance frequency of the dipolar ELSP mode. To illustrate this point, we present our simulation results in **Figure 3b**, which shows that the resonance frequency saturates at the effective surface plasmon frequency as the size of the structure decreases.

We believe that this ELSP-based resonator can be used in the miniaturization of conventional resonators, filters, and other devices operating in the microwave and terahertz frequencies. To which extent this miniaturization can be achieved relies on the fabrication techniques and machining precision. In addition, this resonator is also expected to find many applications as polarization sensors as well.

5. Conclusions

In summary, we have set up the theoretical basis of structural-dispersion-induced effective localized surface plasmons and have derived the analytical description of the modal characteristics of the so-called effective localized surface plasmons. We have also built an open resonator based on these electromagnetic modes which is quite sensitive to the background refractive index, but robust to variations in its size and shape. Experiments are conducted to verify the emergence of effective localized surface plasmons in the microwave regime, and to put the ELSP-based resonator into real sensing applications. We have proven that these effective modes perfectly reproduce the field distributions and evolution characteristics of conventional LSPs in the optical regime. We believe that our findings can find application in the design of novel microwave resonators and filters, as well as sensors operating at higher frequencies, such as the sub-millimeter and terahertz regimes by properly downscaling the structure.

Acknowledgements

Z.L. and L.L. contributed equally to this work. Z.L. acknowledges the financial support from the National Natural Science Foundation of China under Grant No. 61871215, Six talent peaks project in Jiangsu Province under Grant No. 2018-GDZB-009, and Foundation of Key Laboratory of Radar Imaging and Microwave Photonics, NUAA, Ministry of Education under Grant No. XCA17001-05. L.L. and Y.L. acknowledge the financial support from Singapore Ministry of Education Academic Research Fund TIER 1 under Grant No. 2017-T1-001-239 (RG91/17(S)) and TIER 2 under Grant No. MOE2015-T2-1-145. A.I.F.-D. and F.J.G.-V. acknowledge financial support from the Spanish MINECO under Contract Nos. MAT2014-53432-C5-5-R and FIS2015-64951-R, and the “Maria de Maeztu” programme for Units of Excellence in R&D (MDM-2014-0377). A.I.F.-D. also acknowledges funding from EU-FP7 under Grant Agreement No. FP7-PEOPLE-2013-CIG-630996.

Conflict of Interest

The authors declare no conflict of interest.

Keywords

effective localized surface plasmons, parallel plate waveguides, structural dispersion

Received: January 18, 2019

Revised: February 25, 2019

Published online: March 15, 2019

- [1] W. L. Barnes, A. Dereux, T. W. Ebbesen, *Nature* **2003**, 424, 824.
- [2] E. Ozbay, *Science* **2006**, 311, 189.
- [3] T. W. Ebbesen, C. Genet, S. I. Bozhevolnyi, *Phys. Today* **2008**, 61, 44.
- [4] K. A. Willets, R. P. Van Duyne, *Annu. Rev. Phys. Chem.* **2007**, 58, 267.
- [5] N. Fang, H. Lee, C. Sun, X. Zhang, *Science* **2005**, 308, 534.
- [6] M. Ozaki, J. Kato, S. Kawata, *Science* **2011**, 332, 218.
- [7] P. Muhlschlegel, H. J. Eisler, O. J. Martin, B. Hecht, D. W. Pohl, *Science* **2005**, 308, 1607.
- [8] W. Y. Li, P. H. C. Camargo, X. M. Lu, Y. N. Xia, *Nano Lett.* **2009**, 9, 485.
- [9] J. N. Anker, W. P. Hall, O. Lyandres, N. C. Shah, J. Zhao, R. P. Van Duyne, *Nat. Mater.* **2008**, 7, 442.
- [10] J. B. Pendry, L. Martin-Moreno, F. J. Garcia-Vidal, *Science* **2004**, 305, 847.
- [11] A. Pors, E. Moreno, L. Martin-Moreno, J. B. Pendry, F. J. Garcia-Vidal, *Phys. Rev. Lett.* **2012**, 108, 223905.
- [12] A. P. Hibbins, B. R. Evans, J. R. Sambles, *Science* **2005**, 308, 670.
- [13] F. J. Garcia-Vidal, L. Martin-Moreno, J. B. Pendry, *J. Opt. A: Pure Appl. Opt.* **2005**, 7, S97.
- [14] A. P. Hibbins, M. J. Lockyear, I. R. Hooper, J. R. Sambles, *Phys. Rev. Lett.* **2006**, 96, 073904.
- [15] Y. J. Zhou, Q. Jiang, T. J. Cui, *Appl. Phys. Lett.* **2011**, 99, 111904.
- [16] X. Shen, T. J. Cui, D. Martin-Cano, F. J. Garcia-Vidal, *Proc. Natl. Acad. Sci. USA* **2013**, 110, 40.
- [17] X. Gao, J. H. Shi, X. Shen, H. F. Ma, W. X. Jiang, L. Li, T. Cui, *Appl. Phys. Lett.* **2013**, 102, 151912.
- [18] X. Shen, T. J. Cui, *Laser Photonics Rev.* **2014**, 8, 137.
- [19] Z. Liao, X. Shen, B. C. Pan, J. Zhao, Y. Luo, T. J. Cui, *ACS Photonics* **2015**, 2, 738.
- [20] X. Zhang, L. Shen, L. Ran, *J. Appl. Phys.* **2009**, 105, 013704.
- [21] Z. Liao, Y. Luo, A. I. Fernández-Domínguez, X. Shen, S. A. Maier, T. J. Cui, *Sci. Rep.* **2015**, 5, 9590.
- [22] S. J. Berry, T. Campbell, A. P. Hibbins, J. R. Sambles, *Appl. Phys. Lett.* **2012**, 100, 101107.
- [23] P. A. Huidobro, X. P. Shen, J. Cuerda, E. Moreno, L. Martin-Moreno, F. J. Garcia-Vidal, T. J. Cui, J. B. Pendry, *Phys. Rev. X* **2014**, 4, 021003.
- [24] B. J. Yang, Y. J. Zhou, Q. X. Xiao, *Opt. Express* **2015**, 23, 21434.
- [25] S. Kim, S. Oh, K. Kim, J. Kim, H. Park, W. Hess, C. Kee, *Phys. Rev. B* **2015**, 91, 035116.
- [26] L. Liu, L. Wu, J. Zhang, Z. Li, B. Zhang, Y. Luo, *Adv. Sci.* **2018**, 5, 1800661.
- [27] F. Gao, Z. Gao, X. H. Shi, Z. J. Yang, X. Lin, H. Y. Xu, J. D. Joannopoulos, M. Soljačić, H. S. Chen, L. Lu, Y. D. Chong, B. L. Zhang, *Nat. Commun.* **2016**, 7, 11619.
- [28] F. Gao, Z. Gao, Y. Luo, B. L. Zhang, *Adv. Funct. Mater.* **2016**, 26, 8307.
- [29] Z. Liao, A. I. Fernández-Domínguez, J. J. Zhang, S. A. Maier, T. J. Cui, Y. Luo, *ACS Photonics* **2016**, 3, 1768.
- [30] H. C. Zhang, Y. F. Fan, J. Guo, X. J. Fu, T. J. Cui, *ACS Photonics* **2016**, 3, 139.
- [31] J. J. Zhang, Z. Liao, Y. Luo, X. P. Shen, S. A. Maier, *Laser Photonics Rev.* **2017**, 11, 1600191.
- [32] L. L. Liu, Z. Li, B. Z. Xu, C. Q. Gu, J. Xu, C. Chen, H. Y. Sun, Q. X. Xiao, Y. J. Zhou, Q. Qing, P. Shum, Y. Luo, *IEEE Trans. Microwave Theory Tech.* **2017**, 65, 2008.
- [33] P. F. Qin, Y. H. Yang, M. Y. Musa, B. Zheng, Z. J. Wang, R. Hao, W. Y. Yin, H. S. Chen, E. P. Li, *Adv. Sci.* **2017**, 5, 1700487.
- [34] A. Kianinejad, Z. N. Chen, L. Zhang, W. Liu, C. Qiu, *IEEE Trans. Antennas Propag.* **2016**, 64, 2094.
- [35] C. D. Giovampaola, N. Engheta, *Phys. Rev. B* **2016**, 93, 195152.
- [36] Z. Li, L. L. Liu, H. Y. Sun, Y. H. Sun, C. Q. Gu, X. L. Chen, Y. Liu, Y. Luo, *Phys. Rev. Appl.* **2017**, 7, 044028.
- [37] F. R. Prudencio, J. R. Costa, C. A. Fernandes, N. Engheta, M. G. Silveirinha, *New J. Phys.* **2017**, 19, 123017.
- [38] Z. Li, Y. H. Sun, K. Wang, J. J. Song, J. F. Shi, C. Q. Gu, L. L. Liu, Y. Luo, *Opt. Express* **2018**, 26, 4686.